PNAS RESEARCH ARTICLE | ENGINEERING

Investigation of the yielding transition in concentrated colloidal systems via rheo-XPCS

Gavin J. Donley[a,b,c], Suresh Narayanan[d], Matthew A. Wade[a], Jun Dong Park[e], Robert L. Leheny[f], James L. Harden[g], and Simon A. Rogers[a,1]

Edited by David Weitz, Harvard University, Cambridge, MA; received September 9, 2022; accepted February 4, 2023

We probe the microstructural yielding dynamics of a concentrated colloidal system by performing creep/recovery tests with simultaneous collection of coherent scattering data via X-ray Photon Correlation Spectroscopy (XPCS). This combination of rheology and scattering allows for time-resolved observations of the microstructural dynamics as yielding occurs, which can be linked back to the applied rheological deformation to form structure–property relations. Under sufficiently small applied creep stresses, examination of the correlation in the flow direction reveals that the scattering response recorrelates with its predeformed state, indicating nearly complete microstructural recovery, and the dynamics of the system under these conditions slows considerably. Conversely, larger creep stresses increase the speed of the dynamics under both applied creep and recovery. The data show a strong connection between the microstructural dynamics and the acquisition of unrecoverable strain. By comparing this relationship to that predicted from homogeneous, affine shearing, we find that the yielding transition in concentrated colloidal systems is highly heterogeneous on the microstructural level.

yielding | time-resolved rheology | X-ray photon correlation spectroscopy | soft glass | structure–property relations

Significance

The flow and deformation behavior of colloidal glasses are important to a wide range of potential applications, but direct connections between the macroscopic flow/deformation and microscopic structure or dynamics have been difficult to come by. In this work, we utilize simultaneous stress-controlled rheology and x-ray scattering to bridge this gap. By probing the onset of yielding in a colloidal glass, we determine that the transition from recoverable to unrecoverable deformation is strongly linked to the loss of structural memory and the acceleration of the nanoscale fluctuations of the glass.

Glassy dynamics are exhibited by a wide range of soft materials including concentrated colloidal suspensions (1–15) and emulsions (3, 16–20), foams (21–23), and microgels (4, 11, 19, 21, 24, 25). These materials all exhibit a macroscopic yield transition: a process in which the physical behavior transitions from solid-like to fluid-like once the applied deformation or stress passes some critical threshold (26–30). The ability of these materials to yield has resulted in their widespread use in applications as diverse as spreadable foods, personal care products, and materials for additive manufacturing, all of which benefit from the ability to control the fluidity of a material on demand. In order to precisely design novel colloidal systems which exhibit yielding, it is critical to understand the specific physical processes occurring during this transition.

At the continuum level, yielding has been thought of as an instantaneous transition to a flowing state at a fixed stress threshold (27, 29, 31). This view originates from the investigations of plastic flow by Schwedoff (32) and Bingham (31, 33) in the early 20th century, which chose to focus almost exclusively on the steady-state flow of the materials in question. This picture has been clarified by recent studies, which have shown both the importance of elasticity (34) to the process of yielding, and the gradual nature of the transition (24, 25). Additional work has also linked the processes of yielding and unyielding to the loss and formation of material memory in glassy systems (35, 36).

While a range of techniques have been proposed to study the yielding transition (21, 24–27, 30, 33), many assume a Bingham-type yield transition that is instantaneous and are unable to resolve how yielding evolves nor can they distinguish between elastic deformation and plastic or viscous flow in a time-resolved manner. The notable exception is recovery tests (4, 25, 37–40) that separate the applied strain in a rheological test into recoverable and unrecoverable components that are easily interpreted in terms of solid-like or elastic and fluid-like or flow behaviors. Creep and recovery (39) and straining and recovery tests (25) have recently been used to study the onset of the yielding transition by directly probing the reversibility of any deformation, with the transition to unrecoverable flow being linked to the reversible–irreversible transition observed in jammed systems (41–44). These tests have shown that materials begin to acquire strain unrecoverably once the linear regime is exceeded and then transition to steady flow at larger applied deformations. Under oscillatory deformations, the acquisition of unrecoverable strain has also been shown to be closely related to the progression of yielding (4). Despite these advances, a precise definition of when the yielding transition occurs, and the relationship between the unrecoverable strain and any microstructural changes that occur during yielding, remain inconclusive (21, 24, 25, 27).

Author affiliations: [a]Department of Chemical and Biomolecular Engineering, University of Illinois at Urbana-Champaign, Urbana, IL 61801; [b]Department of Physics & Institute for Soft Matter Synthesis and Metrology, Georgetown University, Washington, DC 20057; [c]Infrastructure Materials Group, Materials and Structural Systems Division, Engineering Laboratory, National Institute of Standards and Technology, Gaithersburg, MD 20899; [d]X-ray Science Division, Argonne National Laboratory, Lemont, IL 60439; [e]Department of Chemical Engineering, Sookmyung Women's University, Seoul 04310, Korea; [f]Department of Physics and Astronomy, Johns Hopkins University, Baltimore, MD 21218; and [g]Department of Physics, University of Ottawa, Ottawa, ON K1N 6N5, Canada

Author contributions: G.J.D., S.N., and S.A.R. designed research; G.J.D., S.N., and M.A.W. performed research; S.N. and J.D.P. contributed new reagents/analytic tools; G.J.D., S.N., M.A.W., R.L.L., J.L.H., and S.A.R. analyzed data; and G.J.D., S.N., R.L.L., J.L.H., and S.A.R. wrote the paper.

The authors declare no competing interest.

This article is a PNAS Direct Submission.

[1]To whom correspondence may be addressed. Email: sarogers@illinois.edu.

This article contains supporting information online at http://www.pnas.org/lookup/suppl/doi:10.1073/pnas.2215517120/-/DCSupplemental.

Published April 24, 2023.

From a microstructural perspective, glassy dynamics and yielding are associated with the presence and breaking of jammed configurations that result from interparticle repulsion (5, 6, 15, 17, 43–46). The presence of these interactions leads to significantly slowed dynamics (47–50), and the trapping of microstructural elements in local energy wells. Flow only becomes possible once some minimum energy comparable to the well depth is added into the system. Thermal fluctuations are sufficient to play a role in overcoming these energy barriers when the particles are on the order of nm in size, while approximately μm-sized particles form athermal glasses (3). While this energetic argument has featured in many models of glassy yielding (46, 51–55), the exact connection between these microstructures and their respective yielding dynamics is unclear (4, 21, 24, 29, 53).

To investigate microstructural dynamics of yielding, time-resolved measurements of the changes occurring within the microstructure are necessary. Light scattering (1, 13, 20, 56–61) and microscopy (62) have recently provided significant insight into the dynamics of hard (56–59) and soft (1, 13, 20, 60, 62) glassy materials. In the specific case of colloidal soft glasses, X-ray scattering has been shown to be particularly helpful as it can access structure and dynamics on the scale of nanoparticles (63). While traditional small-angle X-ray scattering (SAXS) can be used to characterize the microstructure of these systems, dynamic information is obtained via X-ray photon correlation spectroscopy (XPCS) (63), which functions analogously to dynamic light scattering (DLS), but accesses nanoscale dynamics with successive SAXS measurements using a coherent beam (64). While XPCS has traditionally been performed on quiescent samples, out-of-equilibrium dynamics can be probed via the application of shear or flow to the material (65–68). For this reason, a combined rheometry/scattering technique (rheo-XPCS) has been recently implemented to facilitate the development of flow-dependent structure–property relations for these systems (69) and has shown promise under both steady shear startup (1) and oscillatory shear (15, 20). In this work, we use rheo-XPCS to investigate the microstructural evolution of concentrated colloidal suspensions using creep/recovery protocols to identify rheological conditions for yielding and demonstrate an intimate connection between the accumulation of unrecoverable strain and how yielding progresses microstructurally.

Results and Discussion

Creep/Recovery Rheology. To assess the flow behavior of a soft glassy material, a series of rheo-XPCS creep/recovery tests (30, 37–40) were performed on a concentrated, disordered suspension of charged silica nanoparticles (Ludox TM-50) that forms a ductile solid (*Materials and Methods* and *SI Appendix* for details). These tests allow us to separate the strain into recoverable and unrecoverable components, while simultaneously observing the effect of shear on the microstructure. While prior XPCS studies have focused solely on the total strain, we focus here on the unrecoverable strain, which has been shown to track the yielding transition (4).

We show in Fig. 1*A* the macroscopic deformation results from the creep and recovery tests performed in this study, focusing on the effect of increasing the creep stress (σ_C) for a fixed creep time (t_C). Three measurement intervals can be distinctly seen: (Q) the quiescence prior to creep; (C) the interval of creep; and (R) the zero-stress recovery step. All measurements begin at zero strain, $\gamma = 0$, under quiescence, with some amount of strain being acquired during the creep step. At a time t_C the stress is set to zero, and the strain is allowed to recover. The partial recovery of the strain indicates acquisition of both recoverable and unrecoverable components, which sum as follows:

$$\gamma(t_C) = \gamma_{rec}(t_C) + \gamma_{unrec}(t_C). \quad [1]$$

The recoverable strain is related to solid-like deformation and the unrecoverable strain is related to fluid-like flow (4, 38). As "flow" corresponds to the acquisition of unrecoverable strain, we can use γ_{unrec} to probe the yielding transition. In Fig. 1*B*, we plot γ_{unrec} against the creep stress for each of the experiments with different values of t_C. At each value of t_C, the value of γ_{unrec} is low (i.e., $<10^{-4}$) at small stresses, and increases approximately linearly with stress above a critical threshold. This critical stress is seen to decrease as t_C increases, ranging from ~30 Pa for $t_C = 1$ s, to ~1 Pa for $t_C = 100$ s. This suggests that the yielding is not exclusively determined by the stress but increases in likelihood as t_C increases. This indicates the possibility of a thermal mechanism for yielding in this system, which is consistent with the fact that our colloidal glass is made up of Brownian particles (~20 nm in diameter). For the purposes of this paper, we will define the yield stress as the critical stress at the shortest creep time [i.e., $\sigma_y = \sigma_{crit}(t_C = 1) \approx 30$ Pa].

Rheo-XPCS.

Two-time correlations. While we can identify a possible yielding point rheologically via the unrecoverable strain, it is not immediately clear whether such a point has any significance to the

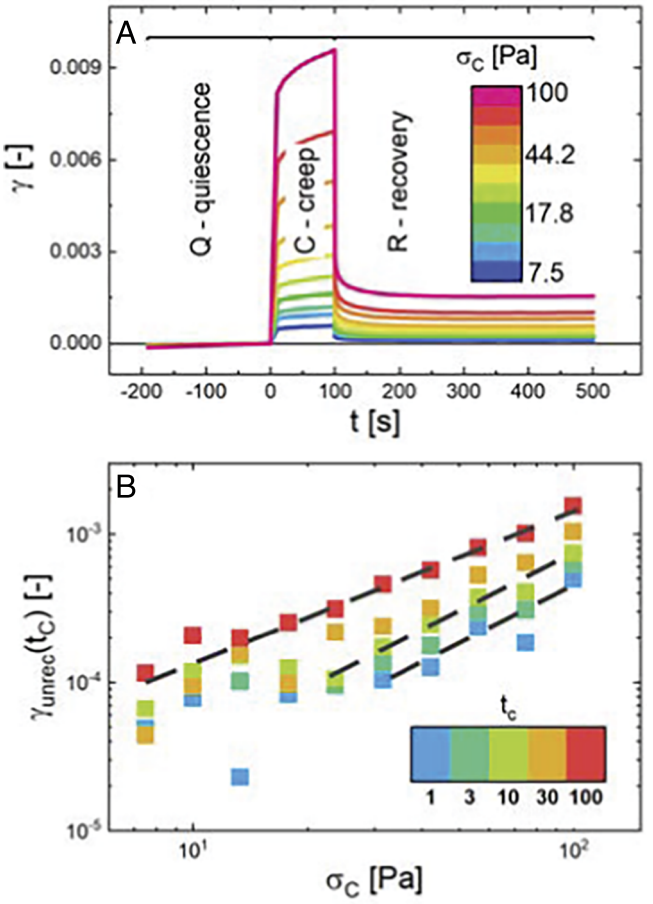

Fig. 1. Rheological measurements on concentrated Ludox TM-50 (~42 vol%): (*A*) Creep/recovery rheology for $t_C = 100$ s. (*B*) Unrecoverable strain for the full set of creep/recovery tests. Dashed lines act as guides to the eye. Some variability is seen between the different creep times.

microscopic structural processes in this colloidal glass. To this end, the XPCS results of two example creep/recovery test cases are detailed in Fig. 2, where σ_C is below yielding (Fig. 2 *A* and *B*) and above yielding (Fig. 2 *C* and *D*), respectively.

To observe the time dependence of the microstructural dynamics, the time-resolved scattering data are displayed as two-time correlation functions (1, 57–59, 70) for each of the stress cases in Fig. 2 *A* and *C*, respectively. These plots act as a map of the correlations ($C(t_1, t_2)$) of the scattering speckle patterns between each pair of measurement times (t_1 and t_2). The minimum possible correlation is one, which indicates negligible similarity in the scattering pattern. These plots are symmetric about the $t_1 = t_2$ diagonal, which represents the self-correlation values for a given sample age. The plot appears as a grid with three distinct intervals along each axis corresponding to the intervals of applied deformation from Fig. 1*A*. Due to the symmetry of the plot, the grids have six unique regions, three on-diagonal regions (Q, C, and R) which show the correlations at different times within a given interval of deformation, and three off-diagonal regions quiescence-creep (Q-C), creep-recovery (C-R), and quiescence-recovery (Q-R) which show the correlations between times in different deformation intervals.

The strongest correlation is seen in the three on-diagonal regions (Q, C, and R), as they are close to the self-correlation line ($t_1 = t_2$). Microstructural dynamics in these regions are observed as a decaying correlation away from the diagonal, which can be described at low shear rates by a stretched exponential decay (1). The dynamics of the system are steady within the region of quiescence (Q), while the creep (C) and recovery (R) regions show time-dependent decorrelation dynamics, caused primarily by transience in shear rate (Fig. 1*A*) and aging of the material. The average correlation within the interval of quiescence (Q) can be expressed as

$$C_Q(t_1, t_2) = 1 + A_Q e^{-(|t_1 - t_2|/\tau_Q)^{n_Q}}, \quad [2]$$

where A_Q is the decay amplitude, $\Delta t = |t_1 - t_2|$ is the delay time, τ_Q is the decorrelation time, and n_Q is the stretching exponent. In all cases, the subscript Q denotes the measure pertaining to the interval of quiescence. As the dynamics during quiescence are stable, A_Q, τ_Q and n_Q all maintain steady values as a function of age (i.e., $(t_1 + t_2)/2$). $\Delta t = \tau_Q$ is shown as a gray dotted line on each part of Fig. 2. In contrast, the time dependence under creep (C) and recovery (R) causes τ and n to vary with the time elapsed in each interval.

There is essentially no correlation between the structures probed in the Q-C and C-R regions, which is consistent with the accumulation of a significant amount of strain during the creep step and its effect on the speckle pattern. In contrast, the Q-R region shows noticeable differences at small and large applied stresses: A significant correlation is seen between the structure before and after creeping for the small stress case (Fig. 2*A*) but is absent in the large stress case (Fig. 2*C*). This indicates that the microstructural configuration from quiescence is maintained when small creep stresses are applied, while significant irreversible microstructural changes occur at larger applied stresses.

Impact of creep on structure. To explore the effect of the applied creep on the evolution of the microstructure, we take a slice of the two-time correlation function at a constant reference time corresponding to immediately prior to application of the stress ($t_2 = 0$, the red line in Fig. 2 *A* and *C*). This effectively defines a time-resolved memory function of the material's precreep microstructure. As the dynamics of this glass result in a structural

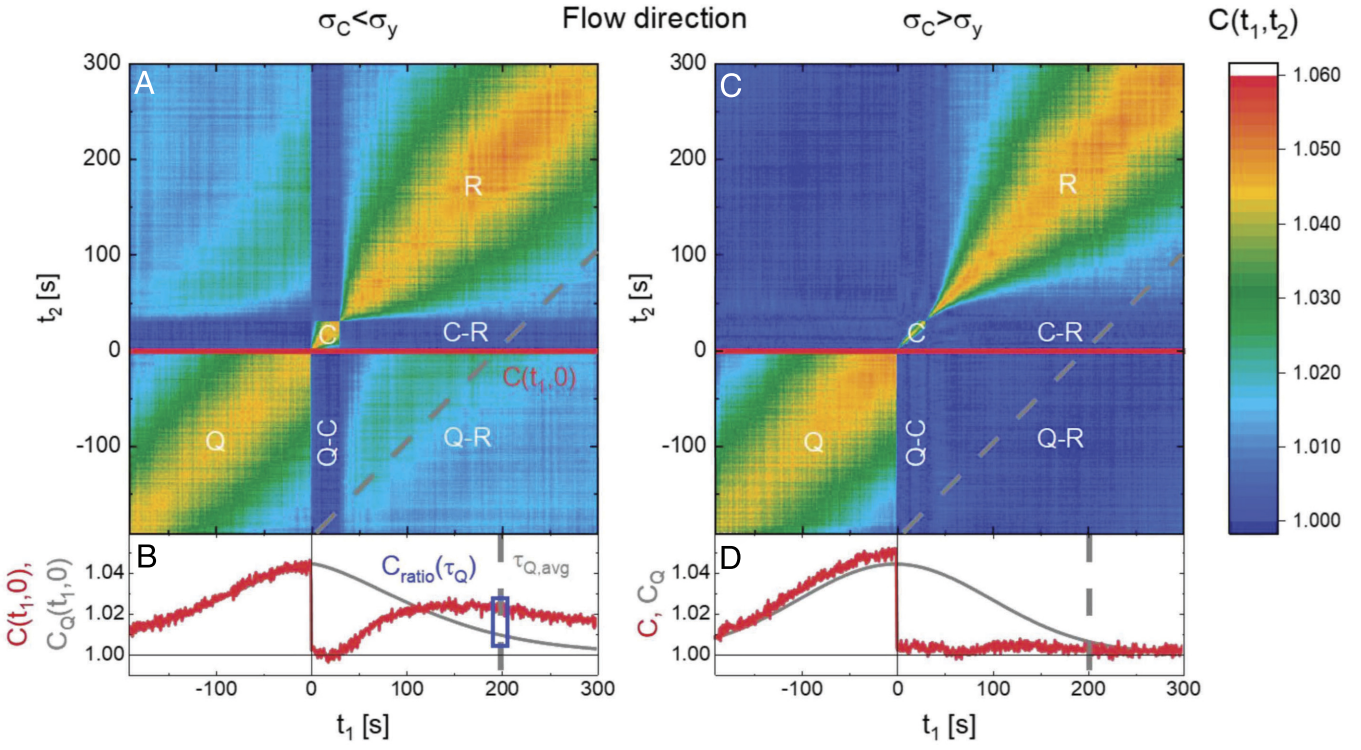

Fig. 2. Rheo-XPCS results: (*A*) Two-time correlation plot from creep/recovery test ($t_C = 30$ s) for small stresses ($\sigma_C = 10$ Pa). The origin in time is chosen as the end of the quiescence interval. The red line corresponds to a cut at constant reference time ($t_2 = 0$). The gray dotted line represents $\Delta t = \tau_q$, the decorrelation time from the quiescent interval (note that only the $t_1 - t_2$ line is shown). The white letters denote the different regions referenced in the text. (*B*) Comparison of a cut at a fixed reference time (red) with the quiescent dynamics of the system (gray) from the small stress case. The blue rectangle denotes the time at which the correlation ratio Eq. **3** is determined. (*C* and *D*) are the corresponding figures for a larger stress case ($\sigma_C = 56.2$ Pa).

memory that fades over time, even without the application of creep to the system, we compare the measured correlation to that of the expected correlation from the average quiescent dynamics Eq. **2** to assess the impact the creep has had on the microstructure.

This comparison can be seen for each applied stress case in Fig. 2 *B* and *D*, respectively. In both cases, the measured correlation in the creep interval drops substantially below the value that would have been observed had creep not been applied, which is indicated by the gray line. At the smaller creep stress, an increase in the structural correlation is seen during the recovery interval, to the point where the measured correlation is larger and decays slower than would be expected from uninterrupted quiescent dynamics. In contrast, the measured correlation increases only minimally at the larger stress once the recovery interval has begun. This comparison suggests the utility of the ratio of actual to quiescent correlation in discerning the yielding response of the sample, incorporating the impact of both memory and dynamics, as proposed in Eq. **3**:

$$C_{ratio}(t_1, t_2 = 0) = \frac{\text{recovery}}{\text{quiescence}} = \frac{C(t_1, t_2 = 0) - 1}{C_Q(t_1, t_2 = 0) - 1}. \quad [3]$$

In this representation, a $C_{ratio} < 1$ indicates an excess of structural dynamics over what would occur without shearing, while a $C_{ratio} > 1$ will occur when the dynamics of the system are slowed. While this ratio is innately time-resolved and defined for all t_1 in the system, we choose to focus on the value of this ratio at the time where $t_1 = \tau_Q$ (i.e., the quiescent decorrelation time). This value ($C_{ratio}(\tau_Q)$) allows us to compare the correlation between structures present at the end of the quiescence interval and a point in the recovery interval which is rigorously defined. Choosing $t_1 = \tau_Q$ for our comparison provides the best balance between allowing sufficient time for the strain to relax while maintaining a value of $C_Q(t_1, 0)$ that is sufficiently large for measurement (C_Q decays with increasing t_1). A comparison of this correlation ratio with the creep/recovery rheology can be seen in Fig. 3.

Fig. 3*A* shows how the value of the measured correlation ratio changes with applied creep stress: C_{ratio} plateaus at the lowest stresses but decreases as the stress increases beyond a value which depends strongly on t_C. This plot is strikingly similar to an inverted Fig. 1*B*, which suggests an anticorrelation between the unrecoverable strain and C_{ratio}. This is further cemented by the fact that the stress where $C_{ratio}(\tau_Q)$ falls below 1 for each creep time is approximately the same as the stress where the onset of significant unrecoverable strain occurs, suggesting that the application of a creep stress sufficient to yield the system has dual consequences: the macroscopic consequence of introducing unrecoverable strain to the system and the microscopic consequence of altering the correlation of the microstructure.

Fig. 3*B* further illustrates the strength of this connection and suggests a constitutive relation connecting the macroscopic (γ_{unrec}) and microscopic (C_{ratio}) consequences of the applied stress quantitatively. At the onset of yielding, this relation incorporates a transition between the behavior in its respective limits. For unrecoverable strains which are significantly large such that $C_{ratio}(\tau_Q) < 1$, there is in inverse relationship between $C_{ratio}(\tau_Q)$ and $\gamma_{unrec}(t_C)$ (purple line in Fig. 3*B*). This relation is expressed as

$$C_{ratio}(\tau_Q) = (\gamma_{[C_{ratio}=1]})/(\gamma_{unrec}(t_C)), \quad [4]$$

where $\gamma_{C_{ratio}=1} = 2.4 \times 10^{-4}$ strain units. In the limit of negligible unrecoverable strain, the correlation ratio plateaus

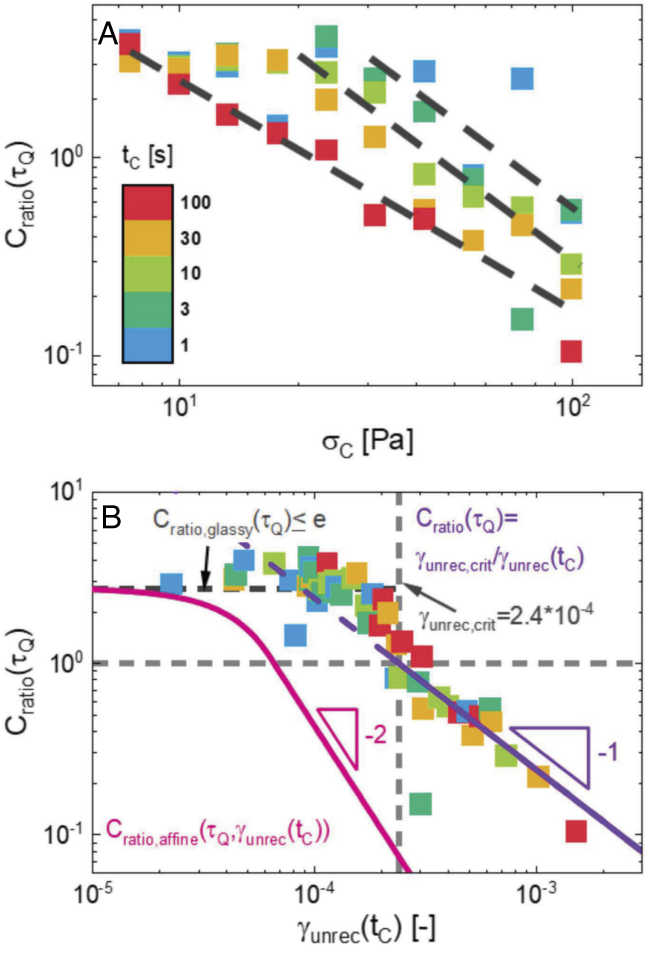

Fig. 3. Comparison of the correlation ratio ($C_{ratio}(\tau_Q)$) to the creep/recovery rheology: (*A*) Comparison to creep stress. Dashed lines are meant to guide the eyes. (*B*) Comparison to unrecoverable strain. Purple line is a fit to the data for $C_{ratio}(\tau_Q) < 1$. Vertical dashed line shows threshold recoverable strain. Pink line shows decay envelope for the predicted $C_{ratio}(\tau_Q)$ assuming perfectly affine strain.

at a value of ~3.5, which is higher than the maximum value obtainable from a simple slowing of dynamics: $C_{ratio,glassy}(\tau_Q) = e \approx 2.72$, indicating increased constraint to the fast, localized motion of the particles in the jammed configuration (details in the *SI Appendix*). This innate connection between the accumulated unrecoverable strain and the correlation of the microstructure across the applied deformation appears to suggest that small amounts of unrecoverable deformation over-age the colloidal system studied here, while larger quantities (consistent with yielding) destroy the memory of the microstructure, as seen in other systems (35, 36).

Evidence for heterogeneous deformation. We compare the measured values of $C_{ratio}(\tau_Q)$ to those that would result if the unrecoverable strain were simply an affine shear deformation (65, 71) (pink line in Fig. 3*B*, details in the *SI Appendix*), and we see that the measured correlations are significantly greater. Further, at large unrecoverable strain, affine deformations would lead to $C_{ratio}(\tau_Q) \sim \gamma_{unrec}(t_C)^{-2}$, in contrast to that predicted by Eq. **4** (purple line in Fig. 3*B*). These differences suggest that the microscopic deformation associated with the unrecoverable strain is heterogeneous, where the irreversible dynamics are confined to portions of the sample, while other

portions experience significantly reduced irreversible changes, resulting in the maintenance of a highly correlated state.

Conclusions

Our creep and recovery rheo-XPCS tests provide sensitive time-resolved macroscopic and microscopic measures of the yielding response of the concentrated colloidal systems probed in this study. The measured rheology demonstrates that the macroscopic flow behavior of these systems is affected by both the magnitude of the creep stress and the time spent under creep, demonstrating that the yielding transition is more complicated than an abrupt transition at a constant stress threshold. The coupled XPCS measurements show this complex dependence on shear history extends to the structural memory and nanoscale dynamics of the material.

We find a strong inverse connection between the accumulation of unrecoverable strain and the correlation of the microstructure before and after yielding. While the unrecoverable strain has previously been connected to the progression of yielding (4), this work indicates that the unrecoverable strain is additionally an appropriate macroscopic measure for characterizing the extent of microscopic changes undergone by the material as yielding progresses, as summarized in the correlation ratio $C_{ratio}(\tau_Q)$.

The behavior of the correlation ratio as a function of γ_{unrec} provides insight into the nature of the microscopic processes responsible for the accumulation of unrecoverable strain. The fact that the correlation ratio scales more weakly with γ_{unrec} than would be expected under affine deformation suggests that the unrecoverable strain is associated with microscopically heterogeneous changes such that surprisingly large correlations in the microstructure persist before and after yielding. Additionally, although the creep is observed to slow the intrinsic dynamics in the glass, the correlation ratio at small unrecoverable strains obtains values even larger than can be explained by slowed dynamics, strongly suggesting that small unrecoverable strains act to constrain positional fluctuations of the particles in the glassy matrix in some way. These observations suggest that the yielding transition in these systems manifests first as a localized hardening with applied stress followed by the onset of heterogeneous, irreversible flow. The incredibly small recoverable strain which acts as the threshold between these two behaviors (i.e., $\gamma_{C_{ratio}=1} = 2.4 \times 10^{-4}$ strain units) corresponds to unrecoverable displacements of the bob on the order of ~48 nm, which are of comparable length scale to the particles in our system. While we do not think that there is necessarily a causal relationship at play between these length scales, we do note that this indicates yielding can occur at very small deformations at the microstructural level.

While we have focused on connecting the rheo-XPCS two-time correlations to simple creep and recovery experiments in this work, similar experiments and analyses on more complicated flow profiles such as oscillatory shear have potential to be equally informative in regard to the coupling of structural memory and dynamics to applied deformation.

Materials and Methods

This study utilizes a concentrated aqueous suspension of colloidal Ludox TM-50 silica nanoparticles with a particle diameter on the order of 20 nm. The resulting sample was a soft repulsive glass with a volume fraction of ~42 vol%, similar to that used in (1, 4, 11, 72). Specific preparation instructions can be found in *SI Appendix*.

The combined rheo-XPCS tests were performed on beamline 8-ID-I at the Advanced Photon Source; details of the beamline setup can be found in *SI Appendix*. All reported correlation values were obtained at the primary peak in the structure factor ($q = 0.0237^{-1}$, $d = 26.5$ nm). The values presented here were also taken exclusively from scattering in the direction parallel to the applied shear, as we aim to directly compare the shear rheology and the microstructure.

In situ rheology was collected via an Anton Paar Physica MCR 301 rheometer. Measurements were taken with a custom 11.4 mm cup/11 mm bob geometry constructed from polycarbonate, to allow for x-ray transmission. The setup was placed inside a polycarbonate enclosure, and the air inside was humidified to reduce sample evaporation.

The rheological protocol consisted of three steps with concurrent scattering: 1) a 200-s zero applied rate interval to probe quiescent dynamics; 2) an interval of creep ($7.5\ \text{Pa} \leq \sigma_C \leq 100\ \text{Pa}$, $1\ \text{s} \leq t_C \leq 100\ \text{s}$); and 3) a 400-s constrained (zero stress) recovery step to separate the recoverable and unrecoverable strains (4, 37, 38, 40). Further rheological details can be found in *SI Appendix*, including a preshear protocol, linear viscoelastic characterization, and offline measurements.

Data, Materials, and Software Availability. The full set of data shown in the manuscript can be accessed via Mendeley Data (https://data.mendeley.com/datasets/65r37w9c8k/1) (73).

ACKNOWLEDGMENTS. We thank Anton Paar for the use of the MCR 702 TwinDrive rheometer for offline measurements through their academic VIP program, and the Zhao lab at UIUC for assistance with sample preparation. We also thank Dr. Piyush Singh and Jiho Choi of UIUC for assistance with experiments. This research was performed at beamline 8-ID-I of the Advanced Photon Source and the Center for Nanoscale Materials, US Department of Energy (DOE) Office of Science User Facilities operated for the DOE Office of Science by ANL (contract No. DE-AC02-06CH11357). This material is based on work supported by NSF Grant No. 1847389 and the Laboratory Directed Research and Development program at Sandia National Laboratories. Sandia National Laboratories is a multimission laboratory managed and operated by National Technology and Engineering Solutions of Sandia LLC, a wholly owned subsidiary of Honeywell International Inc. for the US Department of Energy's National Nuclear Security Administration Contract No. DE-NA0003525. R.L.L. acknowledges funding from NSF Grant No. CBET-1804721. J.L.H. acknowledges the support of the Natural Sciences and Engineering Research Council of Canada (NSERC) through the Discovery Grant Program.

1. Y. Chen, S. A. Rogers, S. Narayanan, J. L. Harden, R. L. Leheny, Microscopic dynamics of stress relaxation in a nanocolloidal soft glass. *Phys. Rev. Mater.* **4**, 035602 (2020).
2. C. Christopoulou, G. Petekidis, B. M. Erwin, M. Cloitre, D. Vlassopoulos, Ageing and yield behaviour in model soft colloidal glasses. *Phil. Trans. R. Soc. A.* **367**, 5051–5071 (2009).
3. M. Dinkgreve, M. A. J. Michels, T. G. Mason, D. Bonn, Crossover between athermal jamming and the thermal glass transition of suspensions. *Phys. Rev. Lett.* **121**, 228001 (2018).
4. G. J. Donley, P. K. Singh, A. Shetty, S. A. Rogers, Elucidating the G'' overshoot in soft materials with a yield transition via a time-resolved experimental strain decomposition. *Proc. Natl. Acad. Sci. U.S.A.* **117**, 21945–21952 (2020).
5. B. M. Erwin, M. Cloitre, M. Gauthier, D. Vlassopoulos, Dynamics and rheology of colloidal star polymers. *Soft. Matter* **6**, 2825–2833 (2010).
6. A. le Grand, D. Vlassopoulos, Effects of particle softness on the rheology and yielding of colloidal glasses. *Rheol. Acta* **47**, 579–590 (2008).
7. T. G. Mason, D. A. Weitz, Linear viscoelasticity of colloidal hard sphere suspensions near the glass transition. *Phys. Rev. Lett.* **75**, 2770 (1995).
8. C. Mayer *et al.*, Asymmetric caging in soft colloidal mixtures. *Nat. Mater.* **7**, 780–784 (2008).
9. K. N. Nordstrom *et al.*, Microfluidic rheology of soft colloids above and below jamming. *Phys. Rev. Lett.* **105**, 175701 (2010).
10. K. N. Pham *et al.*, Multiple glassy states in a simple model system. *Science* **296**, 104–106 (2002).
11. A.-M. Philippe *et al.*, Glass transition of soft colloids. *Phys. Rev. E* **97**, 060401 (2018).
12. P. N. Pusey, W. van Megen, Phase behaviour of concentrated suspensions of nearly hard colloidal spheres. *Nature* **320**, 340–342 (1986).
13. P. N. Pusey, W. van Megen, Observation of a glass transition in suspensions of spherical colloidal particles. *Phys. Rev. Lett.* **59**, 2083 (1987).
14. F. Renou, J. Stellbrink, G. Petekidis, Yielding processes in a colloidal glass of soft star-like micelles under large amplitude oscillatory shear (LAOS). *J. Rheol.* **54**, 1219 (2010).

15. M. C. Rogers *et al*., Echoes in X-ray speckles track nanometer-scale plastic events in colloidal gels under shear. *Phys. Rev. E* **90**, 062310 (2014).
16. C. Bower, C. Gallegos, M. R. Mackley, J. M. Madiedo, The rheological and microstructural characterisation of the non-linear flow behaviour of concentrated oil-in-water emulsions. *Rheol. Acta* **38**, 145–159 (1999).
17. T. G. Mason, J. Bibette, D. A. Weitz, Elasticity of compressed emulsions. *Phys. Rev. Lett.* **75**, 2051 (1995).
18. T. G. Mason *et al*., Osmotic pressure and viscoelastic shear moduli of concentrated emulsions. *Phys. Rev. E* **56**, 3150 (1997).
19. G. Ovarlez, Q. Barral, P. Coussot, Three-dimensional jamming and flows of soft glassy materials. *Nat. Mater.* **9**, 115–119 (2010).
20. M. C. Rogers *et al*., Microscopic signatures of yielding in concentrated nanoemulsions under large-amplitude oscillatory shear. *Phys. Rev. Mater.* **2**, 095601 (2018).
21. M. Dinkgreve, J. Paredes, M. M. Denn, D. Bonn, On different ways of measuring "the" yield stress. *J. Nonnewton. Fluid Mech.* **238**, 233–241 (2016).
22. F. Rouyer, S. Cohen-Addad, R. Hohler, Is the yield stress of aqueous foam a well-defined quantity? *Colloids Surfaces A Physicochem. Eng. Asp.* **263**, 111–116 (2005).
23. A. Saint-James, D. J. Durian, Vanishing elasticity for wet foams: Equivalence with emulsions and role of polydispersity. *J. Rheol.* **43**, 1411–1422 (1999).
24. G. J. Donley, J. R. de Bruyn, G. H. McKinley, S. A. Rogers, Time-resolved dynamics of the yielding transition in soft materials. *J. Nonnewton. Fluid Mech.* **264**, 117–134 (2019).
25. R. R. Fernandes, D. E. V. Andrade, A. T. Franco, C. O. R. Negrao, The yielding and the linear-to-nonlinear viscoelastic transition of an elastoviscoplastic material. *J. Rheol.* **61**, 893 (2017).
26. N. J. Balmforth, I. A. Frigaard, G. Ovarlez, Yielding to stress: Recent developments in viscoplastic fluid mechanics. *Annu. Rev. Fluid Mech.* **46**, 121–146 (2014).
27. H. A. Barnes, The yield stress - a review or '$\pi\alpha\nu\tau\alpha\ \rho o\iota$' - everything flows? *J. Nonnewton. Fluid Mech.* **81**, 133–178 (1999).
28. D. Bonn, M. M. Denn, Yield stress fluids slowly yield to analysis. *J. Nonnewton. Fluid Mech.* **324**, 1401–1402 (2009).
29. D. Bonn, M. M. Denn, L. Berthier, T. Divoux, S. Manneville, Yield stress fluids slowly yield to analysis. *Rev. Mod. Phys.* **89**, 035005 (2017).
30. Q. D. Nguyen, D. V. Boger, Measuring the flow properties of yield stress fluids. *Annu. Rev. Fluid Mech.* **24**, 47–88 (1992).
31. E. C. Bingham, An investigation of the laws of plastic flow. *Bull. Bur. Stand.* **13**, 309 (1916).
32. T. Schwedoff. La rigidite des liquides. *Congre's Int. Phys. Paris* **1**, 478–486 (1900).
33. P. Coussot, Bingham's heritage. *J. Phys. Condens. Matter* **17**, 253 (2005).
34. M. Dinkgreve, M. M. Denn, D. Bonn, "Everything flows?": Elastic effects on startup flows of yield-stress fluids. *Rheol. Acta* **56**, 189–194 (2017).
35. N. C. Keim, J. C. Paulsen, Z. Zerevcic, S. Sastry, S. R. Nagel, Memory formation in matter. *Rev. Mod. Phys.* **91**, 035002 (2019).
36. S. Mukherji, N. Kandula, A. K. Sood, R. Ganapathy, Strength of mechanical memories is maximal at the yield point of a soft glass. *Phys. Rev. Lett.* **112**, 158001 (2019).
37. H. M. Laun, Prediction of elastic strains of polymer melts in shear and elongation. *J. Rheol.* **30**, 459 (1986).
38. J. C. W. Lee, K. M. Weigandt, E. G. Kelley, S. A. Rogers, Structure-property relationships via recovery rheology in viscoelastic materials. *J. Rheol.* **30**, 459 (1986).
39. E. N'Gouamba, J. Goyon, P. Coussot, Elastoplastic behavior of yield stress fluids. *Phys. Rev. Fluids* **4**, 123301 (2019).
40. K. Weissenberg, A continuum theory of rhelogical phenomena. *Nature* **159**, 310–311 (1947).
41. P. Das, H. A. Vinutha, S. Sastry, Unified phase diagram of reversible-irreversible, jamming and yielding transitions in cyclically sheared soft sphere packings. *Proc. Natl. Acad. Sci. U.S.A.* **117**, 10203 (2020).
42. P. Hebraud, F. Lequeux, J. P. Munch, D. J. Pine, Unified study of glass and jamming rheology in soft particle systems. *Phys. Rev. Lett.* **78**, 4657 (1997).
43. G. I. Menon, S. Ramaswamy, Universality class of the reversible-irreversible transition in sheared suspensions. *Phys. Rev. E* **79**, 061108 (2009).
44. K. Nagasawa, K. Miyazaki, T. Kawasaki, Classification of the reversible–irreversible transitions in particle trajectories across the jamming transition point. *Soft Matter* **15**, 7557–7566 (2019).
45. M. E. Cates, J. P. Witmer, J. P. Bouchaud, P. Claudin, Jamming, force chains, and fragile matter. *Phys. Rev. Lett.* **81**, 1841 (1998).
46. A. Ikeda, L. Berthier, P. Sollich, Unified study of glass and jamming rheology in soft particle systems. *Phys. Rev. Lett.* **109**, 018301 (2012).
47. L. Berthier *et al*., Direct experimental evidence of a growing length scale accompanying the glass transition. *Science* **310**, 1797–1800 (2005).
48. D. Brambilla *et al*., Probing the equilibrium dynamics of colloidal hard spheres above the mode-coupling glass transition. *Phys. Rev. Lett.* **102** (2009).
49. L. Cipelletti, L. Ramos, Probing the equilibrium dynamics of colloidal hard spheres above the mode-coupling glass transition. *J. Phys. Condens. Matter* **17**, 253 (2005).
50. L. Ramos, L. Cipelletti, Ultraslow dynamics and stress relaxation in the aging of a soft glassy system. *Phys. Rev. Lett.* **87**, 245503 (2001).
51. M. L. Falk, J. S. Langer, Dynamics of viscoplastic deformation in amorphous solids. *Phys. Rev. E* **57**, 7192 (1998).
52. S. M. Fielding, P. Sollich, M. E. Cates, Aging and rheology in soft materials. *J. Rheol.* **44**, 323 (2000).
53. P. Leishangthem, A. D. S. Parmar, S. Sastry, Effects of particle softness on the rheology and yielding of colloidal glasses. *Nat. Commun.* **8**, 14693 (2017).
54. J. D. Park, S. A. Rogers, The transient behavior of soft glassy materials far from equilibrium. *J. Rheol.* **62**, 869 (2018).
55. P. Sollich, F. Lequeux, P. Hebraud, M. E. Cates, Rheology of soft glassy materials. *Phys. Rev. Lett.* **78**, 2020 (1997).
56. A. Das, P. M. Derlet, C. Liu, E. M. Dufresne, R. Maass, Stress breaks universal aging behavior in a metallic glass. *Nat. Commun.* **10**, 5006 (2019).
57. Z. Evenson *et al*., X-ray photon correlation spectroscopy reveals intermittent aging dynamics in a metallic glass. *Phys. Rev. Lett.* **115**, 175701 (2015).
58. S. Kuchemann, C. Liu, E. M. Dufresne, J. Shin, R. Maass, Shear banding leads to accelerated aging dynamics in a metallic glass. *Phys. Rev. B* **97**, 014204 (2018).
59. M. Luttich *et al*., Anti-aging in ultrastable metallic glasses. *Phys. Rev. Lett.* **120**, 135504 (2018).
60. A. Pommella, A.-M. Philippe, T. Phou, L. Ramos, L. Cipelletti, Coupling space-resolved dynamic light scattering and rheometry to investigate heterogeneous flow and nonaffine dynamics in glassy and jammed soft matter. *Phys. Rev. Appl.* **11**, 034073 (2019).
61. P. N. Pusey, W. van Megen, Dynamic light scattering by non-ergodic media. *Phys. A Stat. Mech. Appl.* **157**, 705–741 (1987).
62. E. D. Knowlton, D. J. Pine, L. Cipelletti, A microscopic view of the yielding transition in concentrated emulsions. *Soft. Matter.* **10**, 6931–6940 (2014).
63. R. L. Leheny, XPCS: Nanoscale motion and rheology. *Curr. Opin. Colloid Interface Sci.* **17**, 3–12 (2012).
64. R. N. Andrews, S. Narayanan, F. Zhang, I. Kuzmenko, J. Ilavsky, Inverse transformation: Unleashing spatially heterogeneous dynamics with an alternative approach to XPCS data analysis. *J. Appl. Crystallogr.* **51**, 35–46 (2018).
65. W. R. Burghardt, M. Sikorski, A. R. Sandy, S. Narayanan, X-ray photon correlation spectroscopy during homogenous shear flow. *Phys. Rev. E* **85**, 021402 (2012).
66. S. Busch, T. H. Jensen, Y. Chushkin, A. Fluerasu, X-ray photon correlation spectroscopy during homogenous shear flow. *Eur. Phys. J. E* **26**, 55 (2008).
67. A. Fluerasu *et al*., Dynamics and rheology under continuous shear flow studied by X-ray photon correlation spectroscopy. *New J. Phys.* **10**, 035023 (2010).
68. A. Fluerasu, A. Moussaid, P. Falus, H. Gleyzolle, A. Marsden, Dynamics and rheology under continuous shear flow studied by X-ray photon correlation spectroscopy. *J. Synchrotron Radiat.* **15**, 378–384 (2008).
69. R. L. Leheny, M. C. Rogers, K. Chen, S. Narayanan, J. L. Harden, Rheo-XPCS. *Curr. Opin. Colloid Interface Sci.* **20**, 261–271 (2015).
70. O. Bikondoa, On the use of two-time correlation functions for X-ray photon correlation spectroscopy data analysis. *J. Appl. Crystallogr.* **50**, 357–368 (2017).
71. T. Narayanan, C. Cheung, P. Tong, W. I. Goldburg, X.-L. Wu, Measurement of the velocity difference by photon correlation spectroscopy: An improved scheme. *Appl. Opt.* **36**, 7639 (1997).
72. S. A. Rogers, J. D. Park, C.-W.J. Lee, Instantaneous dimensionless numbers for transient nonlinear rheology. *Rheol. Acta* **58**, 539–556 (2019).
73. G. Donley *et al*., Dataset for: Investigation of the yielding transition in concentrated colloidal systems via rheo-XPCS. Mendeley Data. https://data.mendeley.com/datasets/65r37w9c8k/1. Deposited 13 April 2023.